Viscoelastic gels of guar and xanthan gum mixtures provide long-term stabilization of iron micro- and nanoparticles

Author's version
Published in
Journal of Nanoparticle Research (2012)
DOI: 10.1007/s11051-012-1239-0
http://dx.doi.org/10.1007/s11051-012-1239-0

VISCOELASTIC GELS OF GUAR AND XANTHAN GUM MIXTURES PROVIDE LONG TERM STABILIZATION OF IRON MICRO- AND NANOPARTICLES

Dingqi Xue[a], Rajandrea Sethi[bc]
[a] DIFIS –Dipartimento di Fisica, Politecnico di Torino, Torino, Italy.
[b] DIATI – Dipartimento di Ingegneria dell'Ambiente, del Territorio e delle Infrastrutture, Politecnico di Torino, Torino, Italy.
[c] Corresponding Author. E-mail: rajandrea.sethi@polito.it; Postal address: DIATI - Politecnico di Torino – Corso Duca degli Abruzzi, 24 - 10129 Torino, Italy; Tel.: +39 011 090 7735; Fax: +39 011 090 7699.

Abstract

Iron micro- and nanoparticles used for groundwater remediation and medical applications are prone to fast aggregation and sedimentation. Diluted single biopolymer water solutions of guar gum (GG) or xanthan gum (XG) can stabilize these particles for few hours providing steric repulsion and by increasing the viscosity of the suspension.

The goal of the study is to demonstrate that amending GG solutions with small amounts of XG (XG/GG weight ratio 1:19; 3 g/L of total biopolymer concentration) can significantly improve the capability of the biopolymer to stabilize highly concentrated iron micro- and nanoparticle suspensions. The synergistic effect between GG and XG generates a viscoelastic gel that can maintain 20 g/l iron particles suspended for over 24 h. This is attributed to (i) an increase in the static viscosity, (ii) a combined polymer structure whose yield stress contrasts the downward stress exerted by the iron particles, (iii) the adsorption of the polymers to the iron surface having an anchoring effect on the particles.

The XG/GG viscoelastic gel is characterized by a marked shear thinning behavior. This property, coupled to the low biopolymer concentration used, determines small viscosity values at high shear rates, facilitating the injection in porous media.

Furthermore, the thermosensitivity of the soft elastic polymeric network promotes higher stability and longer storage times at low temperatures, and rapid decrease of viscosity at higher temperatures. This feature can be exploited in order to improve the flowability and the delivery of the suspensions to the target, as well as to effectively tune and control the release of the iron particles.

Keywords: nanoscale zerovalent iron; Rheology; Yield stress; guar gum; xanthan gum; Groundwater remediation;

Abbreviations

ZVI	Zerovalent iron
NZVI	Nanoscale zero-valent iron
MZVI	Microscale zero-valent iron
GG	Guar gum
XG	Xanthan gum
SBS	Single biopolymer solution
BMS	Biopolymer mixture solution
WLF	Williams-Landel-Ferry theory

Introduction

Nanoscale and microscale zero-valent iron (NZVI and MZVI, respectively) are object of great interest in the fields of groundwater remediation and biomedicine . In the former field of application, the effectivity of zero-valent iron (ZVI) particles has been proven in the degradation or immobilization of a wide variety of contaminants . On the other hand, in medical applications ZVI offers potential advantages over other particles due to their high magnetic moment and can maintain superparamagnetism at larger sizes than their oxides . This mechanism allows for an effective use of ZVI for enhancing magnetic separation, drug delivery and magnetic resonance imaging; in addition, in hyperthermia treatments, these particles have the potential to minimize the amount of injected material in patients and therefore to use safer AC magnetic fields .

Despite the appealing properties of ZVI particles, their employment is often hindered by poor colloidal stability. This limitation can be overcome by suspending the particles in biopolymer solutions, such as guar or xanthan gum (GG and XG, respectively) . GG is a galactomannan obtained from the endosperm of the seeds of *Cyamopsis tetragonolobus*, while XG is an extracellular polysaccharide excreted by the bacterium *Xanthomonas campestris* . These two biopolymers are non-toxic, inexpensive, hydrophilic, stable but biodegradable. Previous studies showed that GG and XG enhance the stability of MZVI and NZVI by adsorbing to the surface of iron and providing steric repulsion among the particles, and by increasing the viscosity of the suspension, therefore slowing the aggregation processes . Furthermore, the shear thinning rheological behavior of ZVI suspensions in biopolymer is advantageous in environmental applications during both the storage and the injection in porous media. During storage, the high static viscosity of the suspension can delay particle sedimentation, while during injection the viscosity decreases at high shear rates, requiring lower pumping pressures .

However, in order to stabilize the significant iron load required for field applications (usually greater than 10 kg/m^3), high biopolymer concentrations are necessary, potentially hindering the degradation in the subsurface. The current study aims at improving the long-term stabilization of ZVI particles dispersion by exploiting the synergistic effect deriving from the mixing of GG and XG . When used separately, the water solutions of each polymer are dominated by viscous behavior . Conversely, when mixed together, they form a viscoelastic gel , which can maintain small particles in suspension even at very low polymer concentrations. The specific objectives of this work are (i) to understand the rheological properties of XG and GG mixtures (at different concentrations, mixing ratios and temperatures) and (ii) to investigate their effectiveness in stabilizing MZVI and NZVI over long periods.

Materials and methods

Zero-valent iron particles

Commercial reactive NZVI (NANOFER 25S or N25S) (Fig. 1a) was supplied as liquid slurries by NANO IRON s.r.o (Rajhrad, Czech Republic). N25S has an average particle size of 50 nm and average surface area of 20 – 25 m^2/g. NZVI was separated from the liquid phase, containing a mixture of organic and inorganic stabilizers, by a series of washing cycles with deionized water followed by centrifugation and sedimentation. After washing, NZVI aggregation and sedimentation were prevented by continuous ultrasonication before mixing with the biopolymer mixtures.

Carbonyl iron powder (B200) was provided by BASF SE (Ludwigshafen, Germany, Fig. 1b) and water atomized iron powder (H4) was supplied by Höganäs AB (Höganäs, Sweden, Fig. 1c). The average particle sizes of B200 and H4 are 4.7 μm and 41μm, respectively.

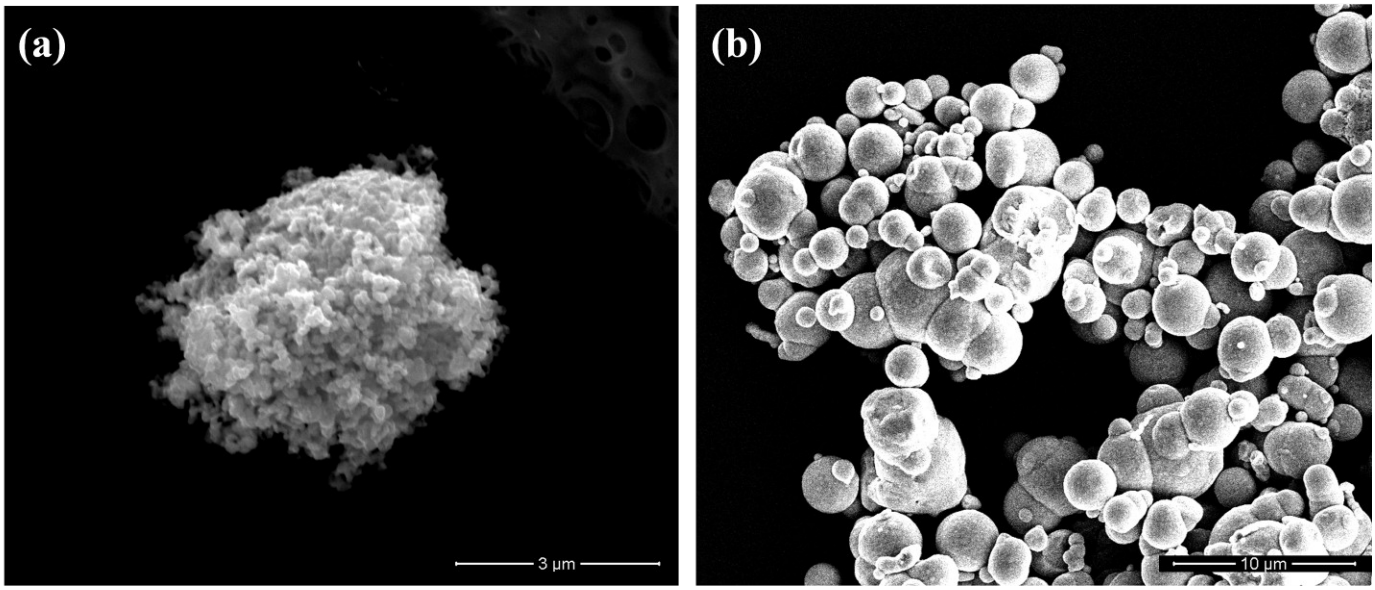

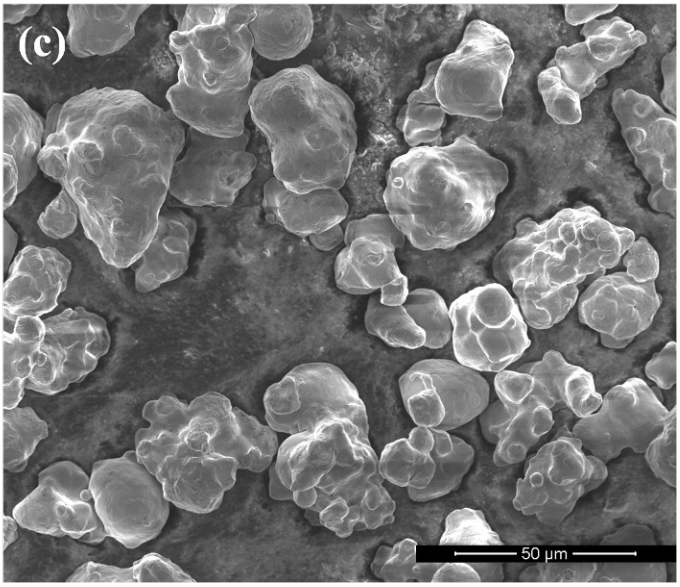

Fig. 1 Representative STEM images of (a) nano iron cluster of N25S, (b) micro iron particles of BASF 200 and (c) micro iron particles of H4

Preparation of biopolymer solutions and ZVI suspensions

Deionized water solutions of XG, GG and their mixtures were stirred firstly with a magnetic stirrer and then homogenized by using the T25 digital Ultra Turrax (IKA, Staufen, Germany) high shear rotor-stator processor. Finally, the biopolymer solutions were degassed under vacuum to remove air bubbles and held for 12 hours at room temperature to facilitate complete dissolution and hydration. ZVI particles were sonicated for 10 mins in deionized water in order to break up the aggregates formed during storage before mixing with biopolymer solutions. The preparation process of ZVI-biopolymer suspensions is schematized in Fig. 2. When preparing ZVI suspensions with biopolymer mixture solution (BMS), as shown by the red arrows, ZVI particles were dispersed firstly in GG solution and then XG solution was added. Suspensions were homogenized by Ultra Turrax homogenizer for 15 mins at 10,000 rpm. The suspensions were ZVI particles (at a concentration of 20 g/L) dispersed in solutions of different polymers (at the concentrations of 6, 3, 2, 1.5 and 0.75 g/L).

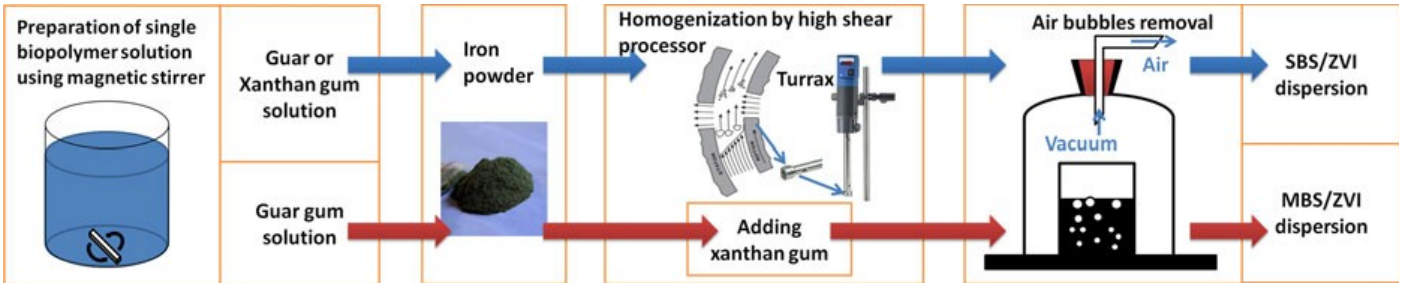

Fig. 2 ZVI-biopolymer suspensions preparation process

Rheology measurements of biopolymer solutions

Dynamic rheological measurements were performed with an Anton Paar MCR-301 rheometer fitted with a concentric cylinder system. The biopolymer microstructure was probed by measuring the shear viscosity, the storage modulus G' (or elastic component), which is a measure of the deformation energy stored by the sample during the shear process, and the loss modulus G" (or viscous component,), a measure of dissipated energy . Dynamic frequency sweeps tests were performed at constant strain amplitude of 1% set within the linear viscoelastic region, which was identified through strain sweep tests. Viscosity was measured as a function of temperature, from 10 ℃ to 40 ℃. Angular frequency sweep tests were conducted between 10 ℃ and 70 ℃ in order to apply the Williams-Landel-Ferry (WLF) theory known as the "time-temperature superposition" which is used to explore fluid rheology in frequency ranges that are otherwise not possible to achieve, neither technically nor practically .

Solutions of XG, GG and their mixture, with concentration values of 6 g/L, 3 g/L and 1.5 g/L and XG/GG weight ratios of 1:4, 2:3, 1:1, 3:2, 4:1 and 1:19, were used in the rheological tests.

The yield stress of the different solutions was determined by measuring the strain while increasing the shear stress in the range from 0.001 to 1 Pa. On a bi-logarithmic stress-strain plot, the yield stress is the point where the relationship between strain and stress deviates from unitary slope. A linear relation with a slope approximately equal to unity implies a Hookean solid-like behavior . In terms of biopolymer structure, this represents the elastic deformation of the structure bonds. When the stress increases over a certain level, some weaker bonds start to break. When the stress exceeds the yield stress, the slope increases significantly and the strain is no longer a function of stress alone, but also depends on the rate of stress increase and duration time. The yield stress represents the transition from elastic solid-like behavior to viscous liquid-like behavior of the biopolymer solutions.

Adsorption of biopolymer molecules

Low-shear viscosity is very sensitive to biopolymer concentration in water, which is decreased by the adsorption to the particle surface.. Differential low-shear viscosity was calculated to estimate the degree of adsorption of XG and GG to the iron surface. Viscosity measurements of XG (at initial concentrations of 3 and 1.5 g/L) or GG (at an initial concentration of 3 g/L) solutions were carried out after the removal by centrifugation of the dispersed ZVI particles (20 g/L), and compared to the viscosity of the same polymer solutions before the addition of ZVI particles.

Sedimentation analysis

Sedimentation tests were used to evaluate the stabilities of N25S, B200 and H4 in XG, GG and their mixture solutions. Sedimentation curves were plotted by exploiting the linear relationship between concentration and magnetic susceptibility, which was logged by a Bartington MS2G susceptivimeter . Susceptibility is an intrinsic property of the material, by measuring the mass susceptibility, the variation of the ZVI's mass over time can be deduced.

Results and discussion

Rheological properties of xanthan gum and guar gum

XG solutions are characterized by a shear thinning behavior, as reported in Fig. 3a. The figure shows the shear rate dependence of viscosity at different polymer concentrations (i.e., 1.5, 3 and 6 g/L) and at different temperatures (i.e., 10, 25 and 40 ℃). The viscosity curve is characterized by a Newtonian region at low shear rates and by a shear thinning behavior at higher shear rates. In this region, the intermolecular interactions are reduced by the micro-structural anisotropy resulting from the shear deformation. As the shear rate increases, the orientation of the polymer chains is forced along the flow direction and produces a drop in the viscosity . Low shear rate viscosity of XG solution is affected markedly by temperature. The structure of the XG molecules changes from a stiff, ordered helical conformation at lower temperatures, to a flexible, disordered structure at higher temperatures . This thermo-rheological behavior is fully reversible between 10 and 70 ℃. The tests also demonstrate that low-shear viscosity increases in a geometric progression when the concentration is doubled (Table 1).

Also GG solutions exhibit a shear-thinning behavior (Fig. 3b). The low-shear viscosity is much lower for GG than for XG solutions; conversely, at high shear rates the viscosity is higher for GG than for XG solutions, at equal concentrations. This is due to the higher molecular weight of XG and to the weaker molecular interactions compared to GG .

Table 1 Low-shear and high-shear viscosities for different biopolymer solutions at 25℃

Shear rate (1/s)	**Viscosity (Pa•s)**											
	XG (3 g/L)	GG (3 g/L)	XG (6 g/L)	GG (6 g/L)	XG/GG =1:19 (1.5 g/L)	XG/GG =1:1 (1.5 g/L)	XG/GG =1:19 (3 g/L)	XG/GG =1:1 (3 g/L)	XG/GG =1:4 (3 g/L)	XG/GG =2:3 (3 g/L)	XG/GG =3:2 (3 g/L)	XG/GG =4:1 (3 g/L)
0.001	5.3	0.16	94	6.1	1	180	28	380	87	87	65	29
1000	0.0097	0.012	0.017	0.041	0.0068	0.0088	0.019	0.018	0.018	0.013	0.012	0.012

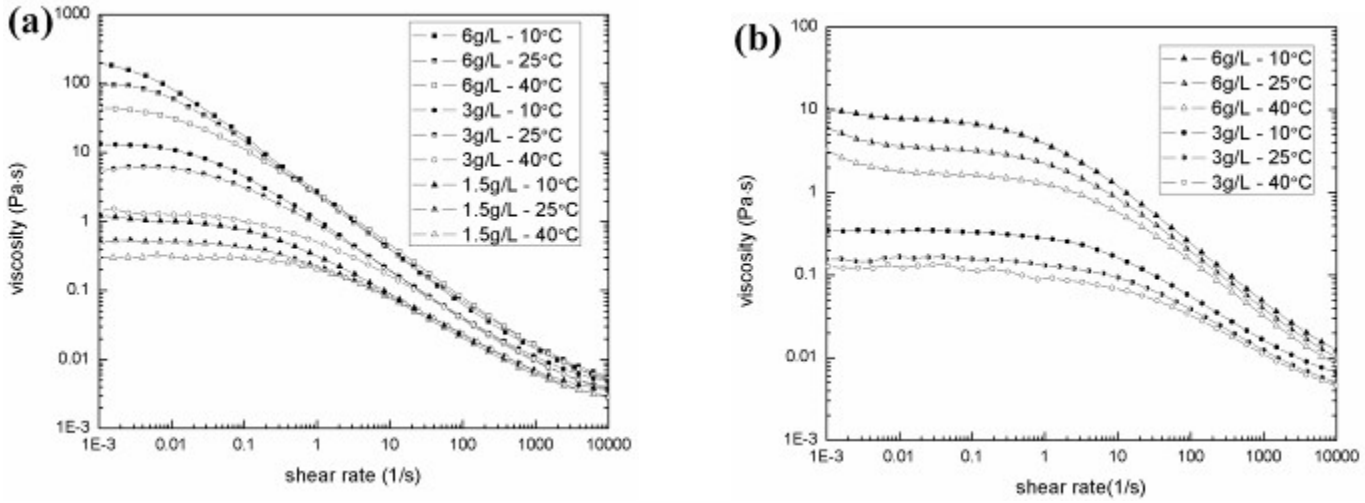

Fig. 3 Viscosity as a function of shear rate at different concentrations and different temperatures for (a) xanthan gum solutions and (b) guar gum solutions

Fig. 4 shows the master curves obtained by sweep tests over a range of angular frequencies for XG and GG solutions at 25℃. By applying the WLF theory, the frequency sweep curves of 10, 25, 40 50 60 and 70℃ between 0.1 and 100 rad/s were converted into one curve at 25℃. The short-term behavior of samples is represented by high frequencies and is dominated by an elastic response when deformation energy is larger than dissipated energy (G'>G"). On the contrary, the long-term behavior is represented by low frequencies and is dominated by a viscous response (G'<G"). The crossover frequency (where G' = G") identifies the transition between solid-like and liquid-like behaviors. The time for a material to adapt to applied stresses or deformations is defined as relaxation time, and is the inverse of the crossover frequency. The curves are influenced by both concentration and temperature. When the concentration increases, both G' and G" increase, and the crossover point shifts to lower frequencies, which means that the elastic behavior is prevailing over the viscous behavior (Table 2).

Fig. 4 shows that a 3 g/L XG solution exhibits an elastic behavior above 0.3 rad/s at 25℃, while for a GG solution at the same concentration G" is larger than G' throughout the frequency range tested. At 6 g/l XG displays a more pronounced elastic behavior than GG. Therefore, frequency sweep tests demonstrate that the structure of XG solutions is more suitable to suspend MZVI and NZVI for longer times than GG solutions at the same concentration.

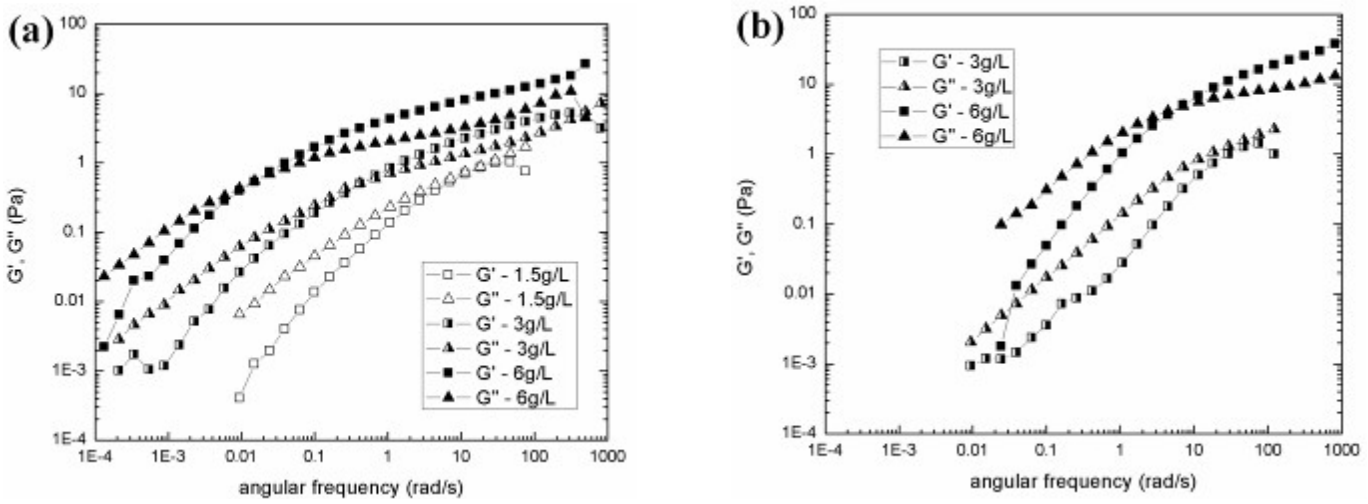

Fig. 4 Master curves of angular frequency sweep measurements determined by the WLF theory at 25℃ for (a) xanthan gum solutions (1.5, 3 and 6 g/L) and (b) guar gum solutions (3 and 6 g/L)

Rheology of BMS

Fig. 5 shows the viscosity curves of BMS with a XG/GG weight ratio of 1:1 at concentration values of 1.5 g/L and 3 g/L at different temperatures. The BMS exhibits a pseudoplastic (shear thinning) behavior affected by temperature, similarly to the parent SBS. Due to the synergistic contribution of the two polymers, the low-shear viscosity of 1.5 g/L BMS with a XG/GG ratio of 1:1 is higher than that of a 6 g/L XG solution (Table 1), while the opposite is true at high shear rates. The extent of the improvement of the rheological properties depends on the mixing ratio between XG and GG. The low-shear (0.001 s^{-1}) and high-shear (1000 s^{-1}) viscosities of BMS (3 g/L) with different mixing weight ratios (i.e., XG/GG ratios of 1:4, 2:3, 3:2, 4:1 and 1:1) and viscosities of single XG and GG solutions at different temperatures are plotted in Fig. 6. At a concentration of 3 g/L, the low-shear viscosities (at a shear rate of 0.001 s^{-1}) of BMS are one to two orders of magnitudes higher than a pure XG solution. As temperature increases from 10℃ to 40℃, these differences decrease. Comparatively speaking, the difference in high-shear viscosity (at a shear rate of 1000 s^{-1}) between BMS and SBS is significantly smaller, which demonstrates that the BMS still possesses favorable flowability. It was also observed that, at relatively low temperatures (i.e., 25℃ and 10℃), the low-shear viscosity is extremely high when the weight ratio of XG/GG is close to 1:1.

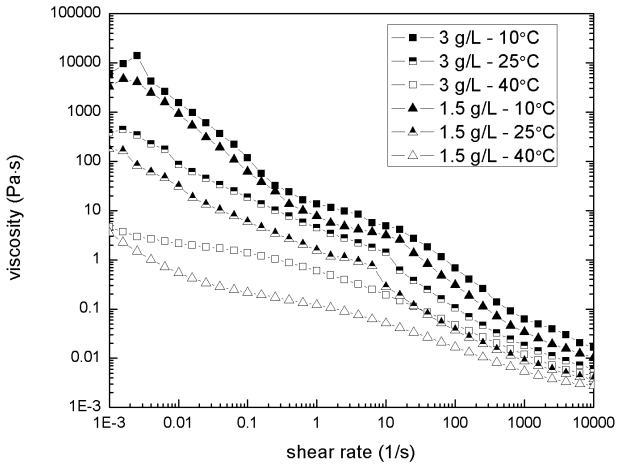

Fig. 5 Viscosity as a function of shear rate for a BMS with a XG/GG weight ratio of 1:1

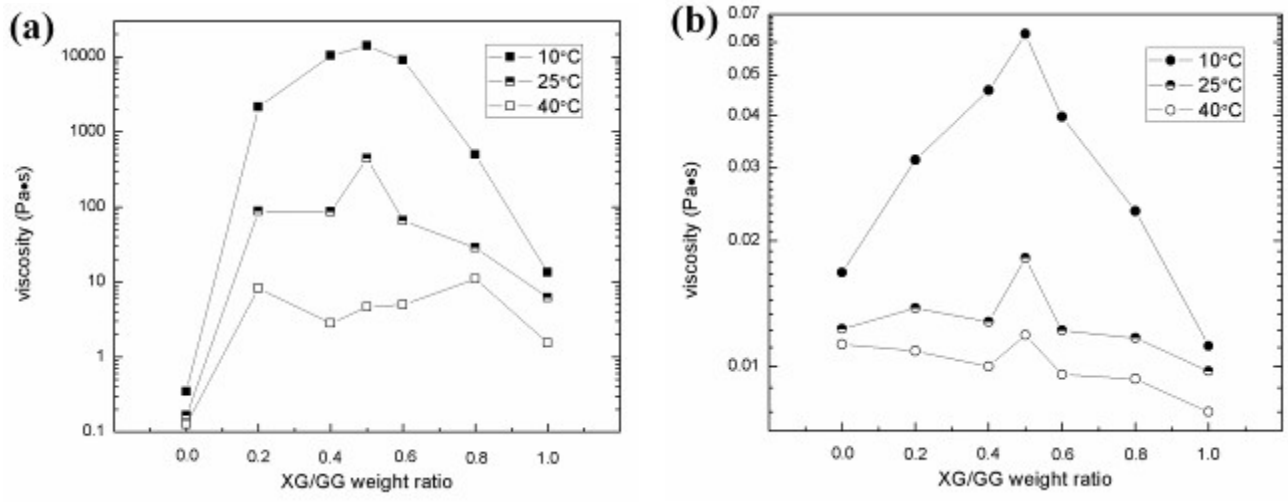

Fig. 6 (a) Low-shear (0.001 s^{-1}) and (b) high-shear (1000 s^{-1}) viscosities of BMS (3 g/L) with different XG/GG weight ratios at different temperatures

Fig. 7 shows the G' and G'' of BMS in frequency sweep tests. Although the G' of a 1.5 g/L BMS with a XG/GG weight ratio of 1:1 is substantially lower than that of a 6 g/L XG solution throughout the frequency range, it is higher than G" at low frequencies (Table 2). The marked elastic behavior of the BMS proves that the interaction between XG and GG generates a much more stable structure than either parent SBS.

Decreasing the XG concentration in the BMS is essential for environmental applications since this polymer is more resilient to biodegradation in aquifer systems and can hinder reactivity of ZVI particles . Fig. 8 and 9 show the rheological properties of a BMS with a XG/GG ratio of 1:19. Although the properties of other mixing ratios (i.e., 1:4, 2:3, 1:1, 3:2 and 4:1) are superior (Table 1), the characteristics of this BMS are still preferable to SBS. For the BMS, the temperature/frequency analogy is not valid and the WLF theory cannot be applied (Fig. 9). The values of the measured moduli are summarized in Table 2. At an angular frequency of 0.1 rad/s (the lowest frequency that can be tested), as the concentration of the SBS decreases, the G'/G" ratio drops

from above to below unity as a result of the weakening of the structure of the fluid. On the contrary, although decreasing concentration reduces both G' and G", the structures of BMS are still characterized by a G'/G" ratio above unity at an angular frequency of 0.1 rad/s, thus are sufficiently stable.

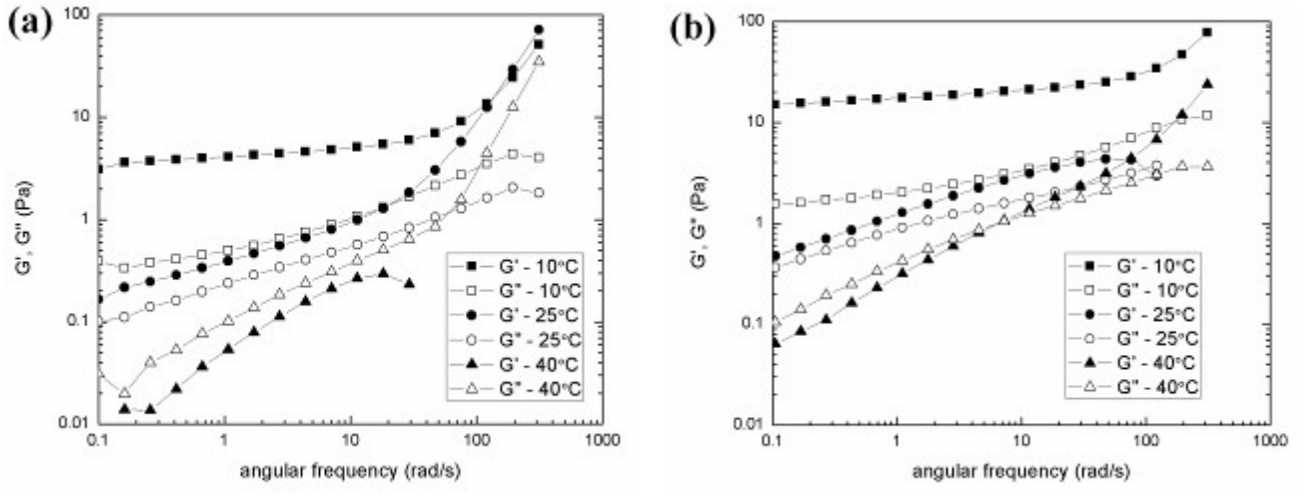

Fig. 7 G' and G'' as a function of angular frequency for BMS with a XG/GG weight ratio of 1:1 at a polymer concentration of (a) 1.5 g/L and (b) 3 g/L

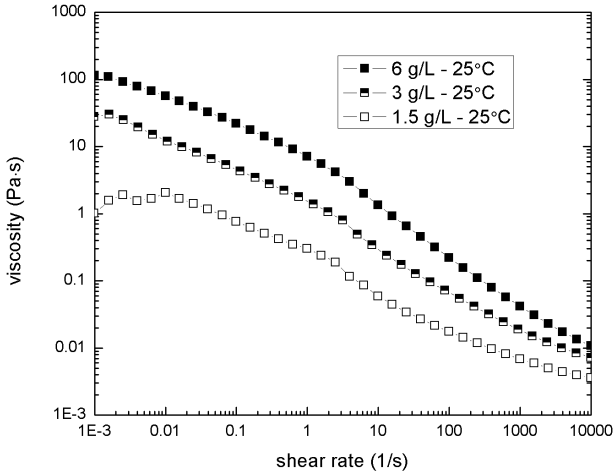

Fig. 8 Viscosity as a function of shear rate for polymer concentrations of 1.5, 3 and 6 g/L with a XG/GG weight ratio of 1:19 at 25℃

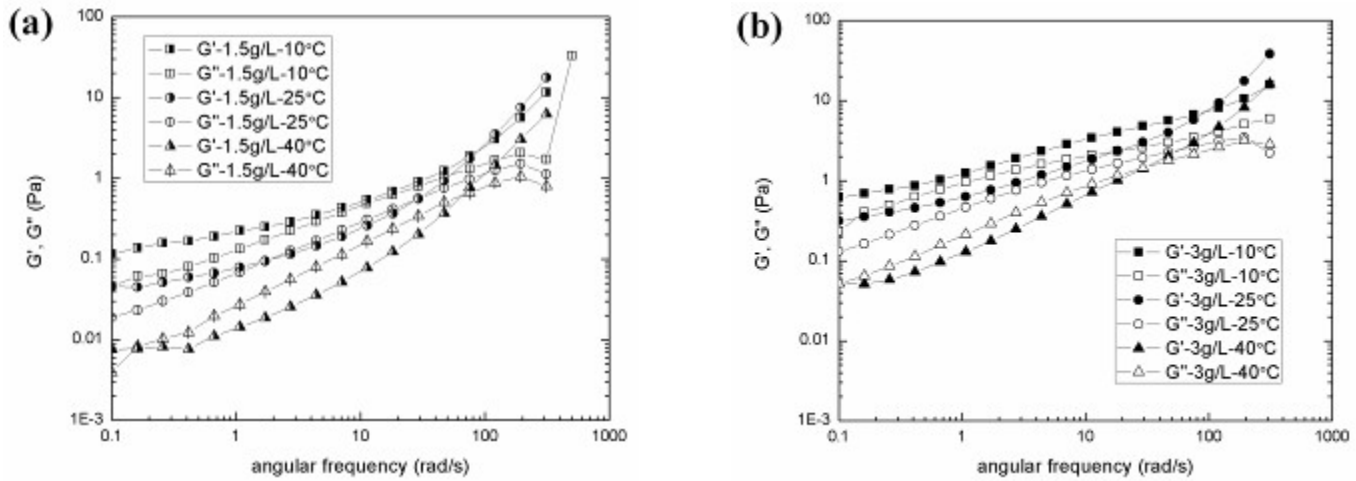

Fig. 9 G' and G" as a function of angular frequency for polymer concentrations of (a)1.5 and (b)3 g/L, with a XG/GG weight ratio of 1:19 at 25℃

Table 2 G' values and its comparison to G'' for different biopolymer solutions at an angular frequency of 0.1 rad/s, at 25℃

	XG (3g/L)	XG (6g/L)	GG (3g/L)	GG (6g/L)	XG/GG=1:19 (1.5 g/L)	XG/GG=1:19 (3 g/L)	XG/GG=1:1 (1.5 g/L)	XG/GG=1:1 (3 g/L)
G' (Pa)	0.189	1.69	0.00358	0.0489	0.0453	0.315	0.166	0.477
G" (Pa)	0.242	1.20	0.00778	0.305	0.0188	0.131	0.103	0.366
Elastic if G'>G"	G' < G"	G' > G"	G' < G"	G' < G"	G' > G"	G' > G"	G' > G"	G' > G"

Temperature dependence of viscosity

Temperature can affect the viscosity of biopolymer solutions due to the change in thermal motion and conformation of the molecules . The temperature dependence of viscosity is reversible and is shown for XG, GG and XG/GG solutions in Fig.10 for different mixing ratios and concentrations. When BMS is characterized by a XG/GG weight ratio of 1:19, or when XG solutions, are heated, viscosity decreases slowly as temperature increases from 10 to 40℃. Instead, when the XG/GG weight ratio ranges from 1:4 to 4:1, and in particular at a ratio of 1:1, low shear viscosity drops sharply in a narrow temperature interval (from 20℃ to 30℃, Fig. 10**)**. This behavior is probably due to the extensive interaction between XG and GG molecules, and to the order-disorder transition of XG molecules from helix to random coil conformation during heating . So the mixture of XG and GG form a thermoreversible soft elastic network structure, which explains why the BMS is gel at low temperatures. This behavior can be exploited to stabilize and store ZVI suspensions at low temperatures and, vice versa, to improve their flowability by heating. A similar strategy can be used to speed up the sedimentation and the release of the particles from the polymer network. Fig. 11 shows how 20 g/L suspensions of H4 and of B200 MZVI dispersed in 1.5 g/L and 0.75 g/L of BMS (XG/GG ratio 1:1), respectively, behave at different temperatures. At 20℃ both the suspensions can be stored without sedimentation for more than 48 h. Nevertheless, when heated to 35℃ and 40℃, respectively, the MZVI settles down within 0.5 h.

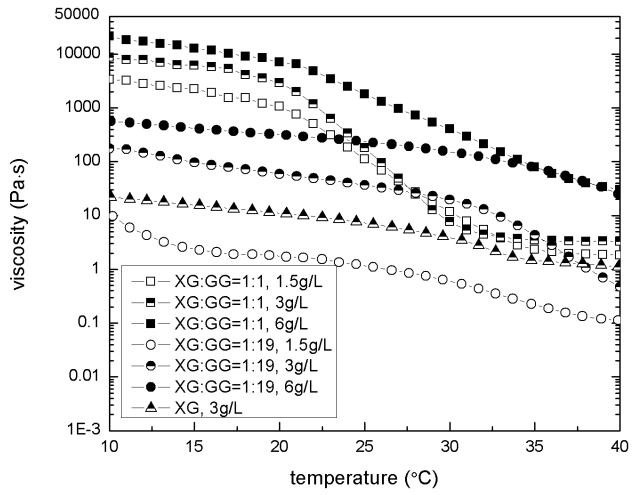

Fig. 10 Viscosity as a function of temperature at a shear rate of 0.001 1/s for different biopolymer solutions

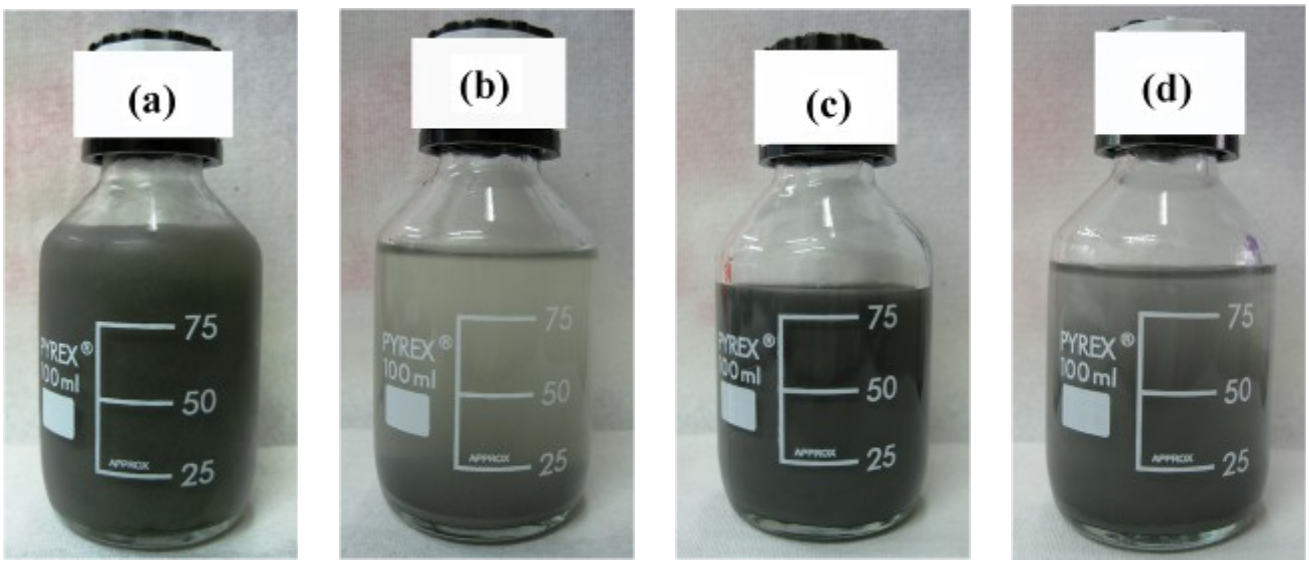

Fig. 11 Thermal effect on sedimentation of 20 g/L MZVI in BMS (XG/GG = 1:1): (a) and (b) H4 in 1.5 g/L BMS at 20℃ after 48 h and at 35℃ after 0.5 h, respectively; (c) and (d) B200 in 0.75 g/L BMS at 20℃ after 48 h and at 40℃ after 0.5 hour, respectively.

Adsorption effect

When ZVI particles are dispersed in XG or GG, they tend to adsorb part of the polymer to their surface, determining a decrease in the viscosity of the suspension thus causing a reduction in its stability. Fig. 12a displays the low shear viscosities of XG or GG solutions before the dispersion of particles and after its removal. It can be clearly seen that the decrease in viscosity of the remnant solution is more significant for smaller particles (N25S and B200) due to their higher specific surface area. High adsorption would lead to an increase of the steric stabilization (especially for NZVI); on the other hand, it would also decrease the solution viscosity and therefore promote sedimentation (particularly of MZVI).

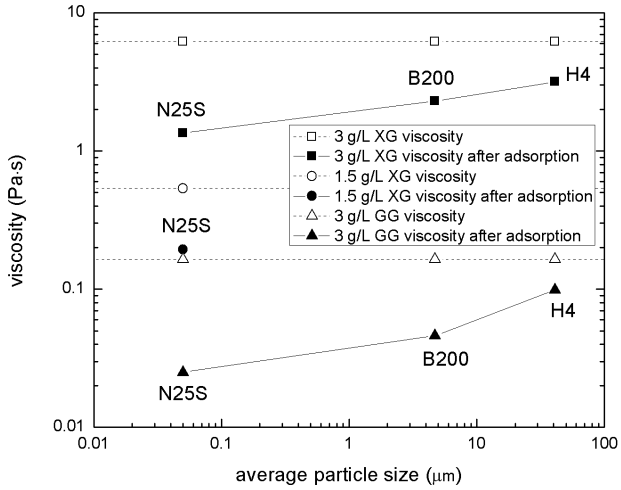

Fig. 12 Viscosity reduction of pure XG and GG solution (3g/L) after adsorption to particles of different sizes at 0.001 1/s shear rate

1. Stability of ZVI particles in polymer solutions

A series of sedimentation experiments proved that ZVI dispersions with diluted SBS (XG or GG) are not stable over long periods of time (Fig. 13). Despite the high static viscosity, XG solutions are not able to stabilize MZVI, which aggregate during sedimentation. The aggregation of MZVI is shown in Fig. 13a-b as an increase of susceptibility normalized to the initial value. During sedimentation, compaction of the iron particles can occur leading to an instantaneous increase of concentration (and susceptibility) when the iron passes by the sensor. Thus, although SBS possesses high low-shear viscosity, the interaction between free biopolymer molecules in solution and those adsorbed to the particle surface is not sufficiently strong to prevent long-term sedimentation as a decrease of susceptibility ratio.

Similarly, Fig. 13c shows that diluted SBS (except XG at 3 g/L) is not able to suspend NZVI for long times. Usually, finer particles are characterized by smaller sedimentation velocity, however, in the 3 g/L GG solution, the NZVI (N25S) settles more rapidly than micro-particles (B200). This is due to the larger specific surface area of NZVI that leads to a higher adsorption of biopolymer with a consequent decrease of the viscosity (Fig. 12a), and to the stronger magnetic interactions occurring among NZVI .

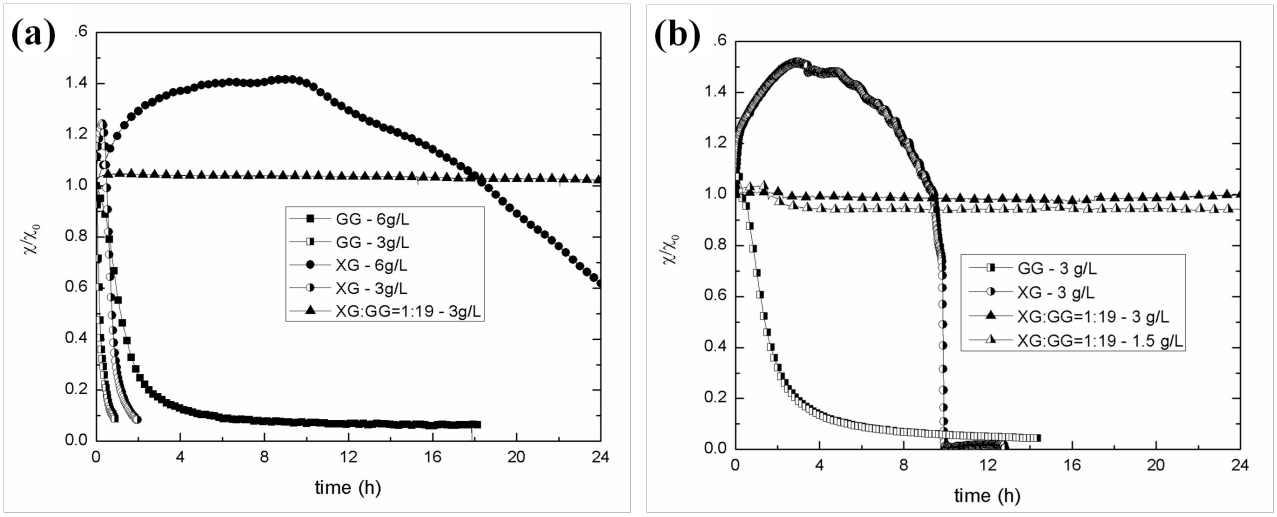

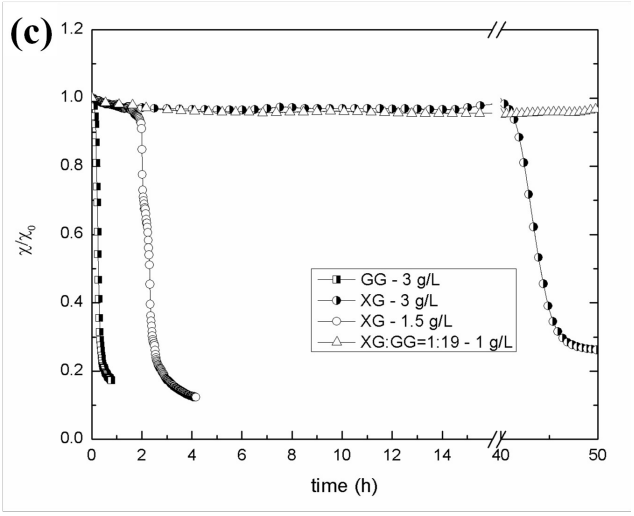

Fig. 13 Sedimentation tests of (a) H4, (b) B200 and (c) N25S dispersed in different biopolymer solutions

The tests performed on SBS proved that the structure of single biopolymers in solution is unable to prevent the sedimentation of ZVI particles due to the unfavorable alignment, and weak interaction among molecules . On the contrary, BMS performs much better than SBS at equal polymer concentration (e.g. 3 g/L), even with a very low XG content (i.e., XG/GG = 1:19, Fig. 13a, b). By comparing the viscosities (Table 1) and the corresponding dispersion stabilities (Fig. 13) of BMS and SBS, the stability of BMS-based ZVI dispersions cannot be attributed solely to the increase of the low-shear viscosity. Despite the smaller low-shear viscosities (0.001 s^{-1}) of BMS with a XG/GG weight ratio of 1:19 at concentrations of 3 g/L, 1.5 g/L and 1 g/L, compared to single XG solutions at 6 g/L, 3 g/L and 1.5 g/L, respectively, their ZVI suspensions are more stable. The structure arising from the mixture of XG and GG can be held responsible for this phenomenon. When XG is dissolved at low temperatures (<40℃), its molecules are present as single, double or triple helices arranged in an ordered conformation that promotes their interaction with the GG molecules . GG consists of a backbone chain of mannose units linked to a monomolecular unit of galactose. Galactose residues are not uniformly distributed: there are regions without galactose (smooth regions) and others with multiple galactose residues (hairy regions). Smooth regions are the ones that favor the interaction with the XG . The interaction between molecules of these gums forms a continuous network structure in BMS, as simply depicted in Fig. 14. Moreover, previous studies showed that GG molecules are able to adsorb to the ZVI surface and that the molecules of both XG and GG have a nanoscale size, with a height of 1.12 nm and a calibrated width of 1.22 nm ; thus, as shown in the schematic representation in Fig. 15 , the GG molecules can be adsorbed to the surface of ZVI particle to form “anchors”, while the xanthan present in the solution provides stability to the biopolymer structure. The presence of a continuous biopolymer gel structure and the adsorption of GG confer a great stability to ZVI dispersed in BMS.

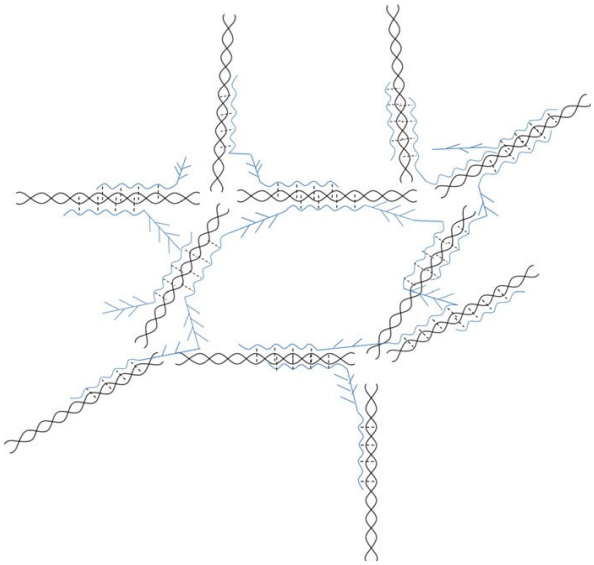

Fig. 14 Schematic representation of the structure formed by the interaction between XG and GG molecules

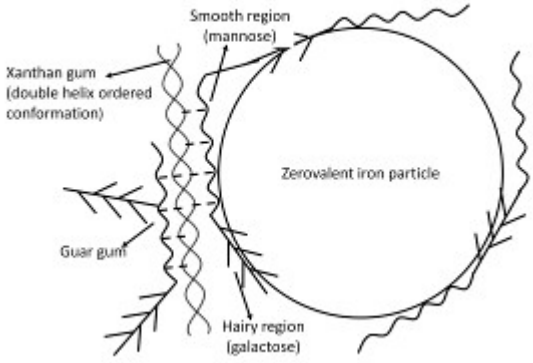

Fig. 15 Schematic representation of interaction among XG, GG and a ZVI particle

The synergetic effect of mixing XG and GG that arises from the formation of a polymeric network structure was verified by yield stress tests. In Table 3 the yield stress of solutions of GG (3 g/L), XG (3 g/L) and BMS (XG/GG = 1:19, 3 g/L) is reported. XG and GG solutions are characterized by a yield stress of 0.12 Pa and 6.58×10^{-3} Pa, respectively; however, when a GG solution is amended with a small amount of XG , the yield stress increases by 2 orders of magnitude. When the yield stress of the polymer solution exceeds the downward stress exerted by the particle, the suspension is stable over long period. Thus, comparing these two stresses can provide a direct evaluation of the effectiveness of polymer solutions in stabilizing suspended particles. The downward stress exerted by an iron particle (Table 3**)** can be calculated according to the expression:

$$\tau = \frac{d}{6}(\rho_p - \rho_f)g$$

where d is the particle diameter, ρ_p is the density of the particles (7900 kg/m^3), ρ_f is the density of the fluid (1000 kg/m^3), g is the acceleration of gravity. The yield and downward stress values are reported in Table 3 and prove quantitatively the efficacy of low-concentration BMS in stabilizing both MZVI and NZVI.

Table 3 Comparison of biopolymer yield stress and particle downward stress and estimation of suspension stability

		Downward stress of iron particle (Pa)		
		H4	B200	N25S
		0.46	5.27×10^{-2}	5.61×10^{-4}
Gel	**Yield stress of polymer solutions (Pa)**	**Yield stress of polymer solutions after partial adsorption on iron (Pa)**		
GG (3g/L)	6.58×10^{-3}	2.37×10^{-3} very unstable	5.11×10^{-4} very unstable	1.51×10^{-4} very unstable
XG (3g/L)	0.123	3.2×10^{-2} very unstable	1.69×10^{-2} Unstable	5.78×10^{-3} stable
XG/GG=1:19 (3g/L)	0.478	0.470 stable	0.443 very stable	0.389 very stable

Conclusions

Previous studies have demonstrated that both GG and XG can improve the stability of concentrated micro- and nanoscale iron particles (e.g., 20 g/l). These polymers can adsorb to the surface of ZVI particle preventing particle aggregation and sedimentation, thanks to an increase in the viscosity of the suspension.

Here, we proposed a strategy to increase the static viscosity of ZVI suspensions while lowering their dynamic viscosity, thus facilitating the injection and flow in porous media, without increasing the polymer concentration. Using low-concentration XG and GG mixtures (XG/GG = 1:19, at 3 g/l) we found that, due to the synergistic interaction of these two gums, a viscoelastic gel is formed, which results in long-term (more than 24 h) stabilization of both the micro- and the nanoscale iron particles at concentrations as high as 20 g/l. . The stabilization effectiveness of this gel was attributed to: (i) the greater static viscosity of the mixture; (ii) the presence of a polymeric structure whose yield stress contrasts the downward stress exerted by the iron particles; (iii) the adsorption of GG molecules to the surface of ZVI particle, which has an anchoring effect on the particles, coupled to the stability provided by the XG to the biopolymeric structure. The marked shear thinning behavior of the BMS and its low biopolymer concentration guarantee low viscosity at high shear rates, facilitating the injection in the subsurface. In addition, the biopolymer mixtures are characterized by a thermoreversible soft elastic network structure, such that the viscosity of the solutions increases at low temperatures and drops suddenly at higher temperatures. This interesting property can be exploited for particles storage at low temperatures, and to improve injection and flowability in porous media at higher temperatures.

Acknowledgments

The work was partially funded by the EU AQUAREHAB research project (FP7, Grant Agreement n. 226565) and by MIUR in the framework of PRIN 2008. The authors acknowledge Dr. M. Coïsson at INRiM for STEM micrographs.

Appendix

G' storage modulus (Pa)

G" loss modulus (Pa)

τ downward stress of particle (Pa)

d average diameter of the particles (m)

ρ_p density of the particles (kg/m^3)

ρ_f density of the fluid (kg/m^3)

g acceleration of gravity (m/s^2)

χ_0 initial mass magnetic susceptibility (m^3/kg)

χ mass magnetic susceptibility (m^3/kg)

References

Amundarain J, Castro L, Rojas M, Siquier S, Ramírez N, Müller A, Sáez A (2009) Solutions of xanthan gum/guar gum mixtures: shear rheology, porous media flow, and solids transport in annular flow. Rheol Acta 48(5):491–498

Born K, Langendorff V, Boulenguer P (2005) Xanthan. In: Biopolymers Online. Wiley-VCH Verlag GmbH & Co. KGaA, Weinheim

Cantrell KJ, Kaplan DI, Wietsma TW (1995) Zero-valent iron for the in situ remediation of selected metals in groundwater. J Hazard Mater 42(2):201–212

Casas JA, Mohedano AF, García-Ochoa F (2000) Viscosity of guar gum and xanthan/guar gum mixture solutions. J Sci Food Agric 80(12):1722–1727

Choppe E, Puaud F, Nicolai T, Benyahia L (2010) Rheology of xanthan solutions as a function of temperature, concentration and ionic strength. Carbohydr Polym 82(4):1228–1235

Comba S, Sethi R (2009) Stabilization of highly concentrated suspensions of iron nanoparticles using shear-thinning gels of xanthan gum. Water Res 43(15):3717–3726

Comba S, Dalmazzo D, Santagata E, Sethi R (2011) Rheological characterization of xanthan suspensions of nanoscale iron for injection in porous media. J Hazard Mater 185(2–3):598–605

Dalla Vecchia E, Coisson M, Appino C, Vinai F, Sethi R (2009a) Magnetic characterization and interaction modeling of zerovalent iron nanoparticles for the remediation of contaminated aquifers. J Nanosci Nanotechnol 9(5):3210–3218

Dalla Vecchia E, Luna M, Sethi R (2009b) Transport in porous media of highly concentrated iron micro- and nanoparticles in the presence of xanthan gum. Environ Sci Technol 43(23):8942–8947

Dea ICM (1989) Industrial polysaccharides. Pure Appl Chem 61(7):1315–1322

Dea ICM, Morris ER (1977) Synergistic xanthan gels. In: Extracellular microbial polysaccharides, ACS symposium series, vol 45. American chemical society, Washington, DC, pp 174–182

Dea ICM, Morris ER, Rees DA, Welsh EJ, Barnes HA, Price J (1977) Associations of like and unlike polysaccharides: mechanism and specificity in galactomannans, interacting bacterial polysaccharides, and related systems. Carbohydr Res 57:249–272

Di Molfetta A, Sethi R (2006) Clamshell excavation of a permeable reactive barrier. Environ Geol 50(3):361–369

Flory PJ (1953) Principles of polymer chemistry. Cornell University Press, Ithaca

Freyria FS, Bonelli B, Sethi R, Armandi M, Belluso E, Garrone E (2011) Reactions of acid orange 7 with iron nanoparticles in aqueous solutions. J Phys Chem C 115(49):24143–24152

García-Ochoa F, Santos VE, Casas JA, Gómez E (2000) Xanthan gum: production, recovery, and properties. Biotechnol Adv 18(7):549–579

Huber DL (2005) Synthesis, properties, and applications of iron nanoparticles. Small 1(5):482–501

Hyun K, Kim SH, Ahn KH, Lee SJ (2002) Large amplitude oscillatory shear as a way to classify the complex fluids. J Nonnewton Fluid Mech 107(1–3):51–65

Iijima M, Shinozaki M, Hatakeyama T, Takahashi M, Hatakeyama H (2007) AFM studies on gelation mechanism of xanthan gum hydrogels. Carbohydr Polym 68(4):701–707

Kim D, Quinlan M, Yen TF (2009) Encapsulation of lead from hazardous CRT glass wastes using biopolymer cross-linked concrete systems. Waste Manag (Oxford) 29(1):321–328

Li X, Elliott DW, Zhang W (2006) Zero-valent iron nanoparticles for abatement of environmental pollutants: materials and engineering aspects. Crit Rev Solid State Mater Sci 31(4):111–122

Mezger TG (2006) The rheology handbook: for users of rotational and oscillatory rheometers. Vincentz Network, Hannover

Milas M, Rinaudo M (1986) Properties of xanthan gum in aqueous solutions: role of the conformational transition. Carbohydr Res 158:191–204

Norton IT, Goodall DM, Frangou SA, Morris ER, Rees DA (1984) Mechanism and dynamics of conformational ordering in xanthan polysaccharide. J Mol Biol 175(3):371–394

Noubactep C, Caré S, Crane R (2012) Nanoscale metallic iron for environmental remediation: prospects and limitations. Water Air Soil Pollut 223(3):1363–1382

Oostrom M, Wietsma TW, Covert MA, Vermeul VR (2007) Zero-valent iron emplacement in permeable porous media using polymer additions. Ground Water Monit Remediat 27(1):122–130

Pai VB, Khan SA (2002) Gelation and rheology of xanthan/enzyme-modified guar blends. Carbohydr Polym 49(2):207–216

Phenrat T, Saleh N, Sirk K, Kim H-J, Tilton R, Lowry G (2008) Stabilization of aqueous nanoscale zerovalent iron dispersions by anionic polyelectrolytes: adsorbed anionic polyelectrolyte layer properties and their effect on aggregation and sedimentation. J Nanopart Res 10(5):795–814

Qiang Y, Antony J, Sharma A, Nutting J, Sikes D, Meyer D (2006) Iron/iron oxide core-shell nanoclusters for biomedical applications. J Nanopart Res 8(3):489–496

Risica D, Barbetta A, Vischetti L, Cametti C, Dentini M (2010) Rheological properties of guar and its methyl, hydroxypropyl and hydroxypropyl-methyl derivatives in semidilute and concentrated aqueous solutions. Polymer 51(9):1972–1982

Rodd AB, Dunstan DE, Boger DV (2000) Characterisation of xanthan gum solutions using dynamic light scattering and rheology. Carbohydr Polym 42(2):159–174

Schramm G, Haake G (1994) A practical approach to rheology and rheometry. Gebrueder Haake, Karlsruhe

Tiraferri A, Sethi R (2009) Enhanced transport of zerovalent iron nanoparticles in saturated porous media by guar gum. J Nanopart Res 11:635–645

Tiraferri A, Chen KL, Sethi R, Elimelech M (2008) Reduced aggregation and sedimentation of zero-valent iron nanoparticles in the presence of guar gum. J Colloid Interf Sci 324(1–2):71–79

Tosco T, Marchisio DL, Lince F, Sethi R (2012) Extension of the Darcy–Forchheimer law for shear-thinning fluids and validation via pore-scale flow simulations. Transp Porous Media 1–20

Truex MJ, Vermeul VR, Mendoza DP, Fritz BG, Mackley RD, Oostrom M, Wietsma TW, Macbeth TW (2011) Injection of zero-valent iron into an unconfined aquifer using shear-thinning fluids. Ground Water Monit Remediat 31(1):50–58

Uhlherr PHT, Guo J, Tiu C, Zhang XM, Zhou JZQ, Fang TN (2005) The shear-induced solid–liquid transition in yield stress materials with chemically different structures. J Nonnewton Fluid Mech 125(2–3):101–119

Wientjes RHW, Duits MHG, Jongschaap RJJ, Mellema J (2000) Linear rheology of guar gum solutions. Macromolecules 33(26):9594–9605

Williams ML, Landel RF, Ferry JD (1955) The temperature dependence of relaxation mechanisms in amorphous polymers and other glass-forming liquids. J Am Chem Soc 77(14):3701–3707

Xiu Z, Jin Z, Li T, Mahendra S, Lowry GV, Alvarez PJJ (2010) Effects of nano-scale zero-valent iron particles on a mixed culture dechlorinating trichloroethylene. Bioresour Technol 101(4):1141–1146

Zhang W (2003) Nanoscale iron particles for environmental remediation: an overview. J Nanopart Res 5(3):323–332

Zhong L, Szecsody J, Oostrom M, Truex M, Shen X, Li X (2011) Enhanced remedial amendment delivery to subsurface using shear thinning fluid and aqueous foam. J Hazard Mater 191(1–3):249–257

Zolla V, Freyria FS, Sethi R, Di Molfetta A (2009) Hydrogeochemical and biological processes affecting the long-term performance of an iron-based permeable reactive barrier. J Environ Qual 38(3):897–908